

1 Ongoing evolution of submarine canyon rockwalls; examples
2 from the Whittard Canyon, Celtic Margin (NE Atlantic)

3
4 **Gareth D.O. Carter^{a*}, Veerle A.I. Huvenne^b, Jennifer A. Gales^c, Claudio Lo Iacono^b,**
5 **Leigh Marsh^{b,d}, Audrey Ougier-Simonin^e, Katleen Robert^b, and Russell B. Wynn^b**

6
7 *^a British Geological Survey, The Lyell Centre, Research Avenue South, Edinburgh, EH14*
8 *4AP, UK*

9 *^b Marine Geoscience, National Oceanography Centre, European Way, Southampton, SO14*
10 *3ZH, UK*

11 *^c University of Plymouth, School of Biological and Marine Sciences, Drake Circus,*
12 *Plymouth, PL4 8AA, UK*

13 *^d Ocean and Earth Science, University of Southampton, Waterfront Campus, Southampton,*
14 *SO14 3ZH, UK*

15 *^e British Geological Survey, Environmental Science Centre, Nicker Hill, Keyworth,*
16 *Nottingham, NG12 5GG, UK*

17 * Corresponding author: gcarter@bgs.ac.uk, +44 131 6500 373.

18
19 **ABSTRACT**

20 During the CODEMAP 2015 research expedition to the Whittard Canyon, Celtic
21 Margin (NE Atlantic), a Remotely Operated Vehicle (ROV) gathered High Definition (HD)
22 video footage of the canyon rockwalls at depths of approx. 412 to 4184 mbsl. This dataset
23 was supplemented by predominantly carbonate rock samples collected during the dives,
24 which were subsequently tested for key physical property characteristics in a geotechnical
25 laboratory. The high-resolution video footage revealed small-scale rockwall slope processes
26 that would not have been visible if shipboard geophysical equipment was solely relied upon
27 during the survey. Of particular interest was the apparent spalling failure of mudstone and
28 chalk rockwalls, with fresh superficial “flaking” scars and an absence of sessile fauna
29 possibly suggesting relatively recent mass-wasting activity. Extensive talus slopes, often
30 consisting of coarse gravel, cobble and occasionally boulder-sized clasts, were observed at
31 the foot of slopes impacted by spalling failures; this debris was rarely colonised by biological

32 communities, which could be an indicator of frequent rockfall events. Bio-erosion was also
33 noted on many of the walls prone to this form of rock slope failure (RSF). As in subaerial
34 equivalents, internal fracture networks appear to control the prevalence of RSF and the
35 geometries of blocks, often resulting in cubic and tabular blocks (0.2-1.0 m scale) of bedrock
36 toppling or sliding out of the cliff face. Tensile strength parameters of carbonate rock
37 samples were determined and these may affect the mass wasting processes observed within
38 the canyon. It was found that carbonate samples which appeared to have a higher mud
39 content, and reduced porosity, produced significantly higher tensile strength values. It is
40 proposed that these stronger, “muddy” carbonate units form the overhanging ledges that often
41 provide an ideal setting for sessile species, such as *Acesta excavata* clams, to colonise
42 whereas the weaker “pure” carbonate units are more easily eroded and therefore form the
43 undercutting, receding sections of the rockwall.

44 By combining the ROV observations, basic discontinuity assessments (estimation of
45 fracture orientations) and laboratory testing results, an understanding of the geomechanical
46 properties of the bedrock can be obtained and linked with past and ongoing rock slope
47 processes within the Whittard Canyon. These conclusions will have a wider implication for
48 ongoing geomechanical processes within submarine canyons on a global scale.

49

50 **Keywords:** submarine canyons, bedrock erosion, bioerosion, canyon rockwalls, Celtic
51 Margin, NE Atlantic, Whittard Canyon, Remotely Operated Vehicle

52

53 1. INTRODUCTION

54 Submarine canyons comprise dynamic environments in which physical and biological
55 processes are constantly altering the slope morphology. The continuous transportation of
56 unconsolidated sediments downslope, and occasionally upslope, by local hydrodynamic

57 forces has been well-documented within submarine canyons (e.g. Cunningham *et al.*, 2005;
58 Puig *et al.*, 2014). Large-scale mass wasting processes and sedimentological down-canyon
59 events such as turbidity currents are known to transport huge volumes of sediment through
60 canyon systems (e.g. Sultan *et al.*, 2007; Lo Iacono *et al.*, 2011; Stewart *et al.*, 2014; Sumner
61 *et al.*, 2014; Talling, 2014).

62 However, there are only limited examples of studies that have investigated the effects
63 of bedrock processes on the morphology of submarine canyons. Despite submarine canyons
64 providing an obvious subaqueous setting where steep, often subvertical or overhanging,
65 bedrock terraces and cliffs are exposed at the seabed, very little research has been devoted to
66 the study of small-scale present-day bedrock erosional processes within these environments
67 and the subsequent consequences for ongoing canyon slope evolution. One example is the
68 study by Micallef *et al* (2012) which presented evidence of deep-seated mass wasting of
69 bedrock slopes within submarine canyons along the active tectonic margin of the Cook Strait,
70 New Zealand. While Micallef *et al* (2012) provided excellent detail on large-scale bedrock
71 landslides, including areas and volumes associated with slope failure events, small-scale
72 bedrock erosional processes and their implications for canyon slope evolution were not
73 discussed.

74 Chaytor *et al* (2016) did present evidence of small-scale bedrock failures within the
75 canyons of the U.S. Atlantic Continental Margin, and linked these processes with structural
76 controls within the bedrock units. However, the geomechanical properties of the different
77 lithological units were not investigated in detail, and the influence of engineering
78 characteristics (e.g. strength or porosity) upon bedrock slope erosion were not expanded upon
79 with quantitative data. McHugh *et al* (1993) provide a detailed study on the role of
80 diagenesis in the exfoliation of carbonate rocks within submarine canyons of the U.S.
81 Atlantic Continental Margin (offshore New Jersey). Visual observations of bedrock erosion,

82 associated with joint network propagation due to diagenetic transformation, were linked with
83 data collected by thin-section, scanning electron microscope/energy dispersive x-ray
84 (SEM/EDX) analyses. However, as with Chaytor *et al* (2016), geomechanical properties
85 were not investigated using geotechnical testing methods.

86 Previous studies from similar geological settings (e.g. Paull *et al* (1990a) focusing on
87 subvertical to vertical limestone cliffs of the Florida Escarpment) have highlighted evidence
88 of ongoing rock slope collapse. This suggests that the present-day slope profile of many
89 subaqueous bedrock terraces and cliffs may have been altered over time by modern erosional
90 processes.

91 External factors can also contribute to the erosion of canyon slopes, with bioerosion
92 linked to benthic faunal communities being one source. A study by Dillon and Zimmerman
93 (1970) in two New England submarine canyons identified outcrops of sandstone, siltstone
94 and semi-consolidated mud that were riddled with burrows measuring up to 50 cm in
95 diameter, which were often occupied by crustaceans such as crabs. Bioerosion of this nature
96 has been noted in other U.S. submarine canyon systems (e.g. Warme *et al.*, 1978; Valentine
97 *et al.*, 1980).

98 Large-scale slope failures, such as those described by Micallef *et al* (2012), and
99 downslope sediment transfer processes (e.g. turbidity currents), as detailed by Sumner *et al*
100 (2014), are known to transfer sediments from upper canyon realms down towards the canyon
101 thalweg. However, what has not been well-documented to-date is the influence that small-
102 scale bedrock erosional processes can have upon canyon dynamics in relation to inducing
103 alterations to the geomorphology. In addition, when discussing mass transfer processes and
104 sedimentary budgets within submarine canyons (e.g. Puig *et al.*, 2003), bedrock erosional
105 processes have frequently been overlooked as a source of seafloor material within canyon
106 systems.

107 Many questions remain unanswered in relation to these erosional mechanisms; what
108 processes are contributing to bedrock erosion in submarine canyons? What role do the
109 geomechanical properties of different lithologies play in promoting ongoing slope erosion?
110 To what extent do benthic faunal communities influence the morphology of submarine slopes
111 and cliffs, including acting as a catalyst for slope erosion within canyon environments as
112 suggested by several authors (e.g. Rowe, 1974; Hecker, 1982)?

113 Here we provide detailed video evidence collected during multiple Remotely
114 Operated Vehicle (ROV) dives, highlighting small-scale present-day processes acting upon
115 bedrock slopes within the Whittard Canyon, Celtic Margin. Measurement of the physical
116 properties of rock samples collected from the canyon walls provide quantitative data, which
117 are used to investigate the impact of bedrock structures and lithology on slope stability. The
118 implications of these results on slope morphology and benthic habitats are discussed in the
119 context of the Whittard Canyon, and more widely in terms of subaqueous rockwalls on a
120 global scale.

121

122 **2. GEOLOGICAL SETTING**

123 The Whittard Canyon is a large dendritic canyon system extending from the shelf
124 edge (approximately 200 m below sea level (mbsl)) to the base of the continental slope at
125 approximately 4500 mbsl. It forms one of the most westerly of a number of submarine
126 canyon complexes located along the passive Celtic Margin (NE Atlantic), approximately 300
127 km SSW of the Republic of Ireland (Figure 1). The continental slope has an average gradient
128 of 8° in the vicinity of the Whittard Canyon, although it varies greatly across the Celtic
129 Margin due to multiple gully and canyon incisions (Amaro *et al.*, 2016). Towards the Goban
130 Spur Margin, which bounds the western extent of the Whittard Canyon complex, the
131 continental slope becomes more laterally continuous with an absence of slope incisions.

132 **FIGURE 1 – FULL PAGE (FIGURE AND CAPTION AT END OF**
133 **MANUSCRIPT)**

134 Laterally, this abrupt change in slope morphology is heavily influenced by changes in
135 the underlying geological structure along the margin. However, the boundary between
136 continental and oceanic crust consistently controls the base of the slope throughout the
137 region, at approximately 4500 mbsl (Evans, 1990). The canyon itself was incised through
138 retrogressive mass wasting of the slope and headwall, instigated during the Pliocene –
139 Pleistocene (Amaro *et al.*, 2016). Although it has previously been noted that there is very
140 little or no evidence of present-day incision of the main axial channel (e.g. Stewart *et al.*,
141 2014; Amaro *et al.*, 2016), the evidence presented in this paper will demonstrate that the
142 major bedrock units that form canyon rockwalls are in no way inert and erosional processes
143 are ongoing.

144 The Early Cretaceous rifting episode of the North Atlantic resulted in the fault-block
145 topography upon which the Celtic Margin formed. These rotated fault-blocks are thought to
146 have influenced the profile of the lower slope, however the present day bathymetry of the
147 upper slope is the result of erosional processes (e.g. slumping and sediment density currents)
148 acting against the continued advancement of the shelf edge by sediment deposition (Evans,
149 1990).

150 The post-rifting stratigraphy comprises Cretaceous chalk, Paleogene limestones and
151 mudstones, and Neogene calcareous clays, calcilutites (Jones Formation) and calcarenites
152 (Cockburn Formation), capped by Pliocene to Pleistocene sediments of the Little Sole
153 Formation (Evans & Hughes, 1984; Evans, 1990; Stewart *et al.*, 2014). No borehole logs
154 were available for the area of the shelf that immediately surrounds the canyon; however,
155 British Geological Survey (BGS) and Deep Sea Drilling Project (DSDP) cores provide a
156 general overview of the stratigraphy for the wider continental shelf and slope (Figure 1

157 (inset)). The Cretaceous chalks logged in BGS borehole +49-009/42 (Figure 2a), located
158 approximately 118 km NE (shelfward) of the canyon head, are described as being white to
159 pale grey, soft to firm, granular and glauconitic in places, and fossiliferous. Sporadic flint
160 nodules are also noted. Elsewhere, DSDP cores (Figure 2b) record carbonaceous and marly
161 nannofossil chalks of Cretaceous age (Montadert *et al.*, 1979). Paleogene soft clays, firm to
162 hard (and glauconitic in parts) limestone and fine-grained carbonaceous sandstone are present
163 in BGS borehole +49-009/42, overlain by Neogene clays that are calcareous, glauconitic,
164 carbonaceous and fossiliferous in nature. The DSDP borehole logs reveal siliceous
165 mudstones, silicified limestones, marly nannofossil chalks and nannofossil ooze of Paleogene
166 age, overlain by Neogene nannofossil chalks and oozes, siliceous mudstones, capped by
167 Pleistocene calcareous muds and nannofossil oozes (Montadert *et al.*, 1979). While these
168 borehole locations are not immediately adjacent to the Whittard Canyon, the formations
169 logged in these cores present a stratigraphic framework for the wider Celtic Margin into
170 which the canyon is incised.

171 The oceanographic conditions of the Celtic Margin are characterized by high-energy
172 hydrodynamics, and tidal currents of up to 0.9 m s^{-1} have been recorded to the southeast of
173 the Whittard Canyon (around La Chapelle Bank), although these decrease to 0.2 m s^{-1} to the
174 northwest around the Goban Spur (Stewart *et al.*, 2014). These large tidal currents are
175 associated with equally large internal tides, guided through the major limbs of the canyon by
176 the seafloor topography (Aslam *et al.*, 2017). Near-bottom current velocities are intensified
177 along the canyon floor, highlighting the influence of canyon topography, and can lead to high
178 concentrations of suspended particles (Aslam *et al.*, 2017; Hall *et al.*, 2017). Along the Celtic
179 Margin, the strengthening of bottom current velocities affects sediment erosion at depths of
180 400 – 500 m (Cunningham *et al.*, 2005). The hydrodynamics across the wider region are
181 known to transport sediments from the near shore, across the shelf and down the margin slope

182 (Stewart *et al.*, 2014). Towards the head of the Whittard Canyon, a series of large (up to 55
183 m high and 200 km long) linear sand ridges were formed between 10 – 20 cal ka, orientated
184 perpendicular to the shelf break (Scourse *et al.*, 2009). These sand ridges, and sandwave
185 fields shelfward of the canyon head, provide a source of sediment for modern transport
186 processes. Present-day down-slope gravity flows have also been noted to transport sediment
187 from the shelf edge down through the canyon (Amaro *et al.*, 2016), and contour currents are
188 responsible for along-slope transport of sediments across the Celtic Margin (Stewart *et al.*,
189 2014).

190 **FIGURE 2 – HALF PAGE (FIGURE AND CAPTION AT END OF**
191 **MANUSCRIPT)**

192
193 **3. DATA AND METHODS**

194 Rock samples and video images from the canyon walls were collected over a four-
195 week period during Expedition JC125 as part of the CODEMAP 2015 project (COMplex
196 Deep-sea Ecosystems: Mapping habitat heterogeneity As Proxy for biodiversity), funded by
197 the European Research Council (Grant No. 258482), onboard the *RRS James Cook*.

198 Videos were collected over 17 dives, from depths of approx. 412 to 4184 mbsl, by the
199 Natural Environment Research Council's (NERC) *Isis* ROV, a science-class system that has a
200 maximum dive depth of 6500 mbsl (Huvenne *et al.*, 2016). The *Isis* ROV uses two different
201 navigation systems; a Sonardyne Ultra-Short Base Line system (USBL) and a Doppler
202 Velocity Log (DVL) dead-reckoning (Huvenne *et al.*, 2016). The video imagery was
203 collected using three optically corrected High-Definition (HD) cameras which were mounted
204 to the front of the ROV; one camera was used primarily for piloting the vehicle, another
205 camera was operated (pan, tilt and zoom functions) by members of the science party during

206 dive operations, and the third camera was kept on a fixed angle and zoom level (Huvenne *et*
207 *al.*, 2016).

208 In addition to the video footage, the ROV collected seven carbonate rock samples
209 (representative of the lithology at each particular dive depth) which were suitable for strength
210 testing using point load test (PLT) and uniaxial compressive strength (UCS) methods (ASTM
211 Standards D5731–5795, 2001, and D2938-95, 2002, respectively). Due to the volume and
212 standard dimensions of material required for UCS testing, only one rock sample recovered by
213 the ROV was suitable for this method. The samples had average dimensions of 218.7 mm x
214 147.6 mm x 65.9 mm, and were acquired from the base of terraces and cliffs that exhibited
215 erosional scars (Figure 1). The highly brittle nature of the mudstones prevented the ROV
216 from obtaining a sample of this lithology. A single sample was acquired from a bioturbated
217 muddy terrace within the thalweg of the western branch; this sample was classified as a soil
218 sample in engineering property terms. All tests were conducted at room temperature,
219 following the ISRM suggested methodologies (Franklin, 1985; Fairhurst and Hudson, 1999;
220 Ulusay and Hudson, 2007) and ASTM standards (ASTM Standards: D4318-10, 2000;
221 D5731–5795, 2001; D2938-95, 2002; D3148-02, 2002; D4543-04, 2004) taking into account
222 the limited material available. The carbonate rock specimens were tested both oven dried and
223 wet using distilled water.

224 **FIGURE 3 – FULL PAGE (FIGURE AND CAPTION AT END OF**
225 **MANUSCRIPT)**

226
227 **4. RESULTS**

228 **4.1 BEDROCK SLOPE PROCESSES**

229 Evidence of active erosion was observed at various depths and across a variety of
230 different bedrock lithologies. The most prevalent of these processes was the widespread

231 exfoliation or spalling failure of vertical to subvertical cliff and terraced surfaces (Figure 3a
232 & b). The most significant erosion was noted in areas of apparently weak mudstone,
233 although occurrences of exfoliation were also noted on carbonate and chalk surfaces (Figure
234 3c). Typically, flakes or cobbles of mudstone were noted to have produced significant
235 accumulations in the form of talus deposits at the base of terraces and cliffs. The exposed
236 face above these talus slopes exhibits patches of fresh, light grey, scar surfaces often adjacent
237 to brown, weathered surfaces unaffected by recent spalling (Figure 3b). The detritus forming
238 the talus slopes is predominantly angular in shape, and composed of generally cobble to
239 occasionally boulder sized clasts, with the surfaces of these slopes being notably devoid of
240 any established benthic communities (Figure 3d). On the carbonate (predominantly chalk)
241 units, shallow exfoliation of the exposed surface was visible in the form of flaked patches of
242 fresh, bright white scars (devoid of benthic fauna) adjoining areas of beige, weathered
243 surfaces that were often colonized by sessile fauna (Figure 3c).

244 Active retreat of terraced mudstone slopes through spalling erosion was noted on 11
245 separate occasions over the course of the 17 ROV dives (Figure 3a & b). Additionally, the
246 undermining of basal sections of mudstone terraces through localized spalling failure and
247 bioerosion was observed (Figure 3b).

248 In addition to spalling failure, evidence of block failure was observed in mudstone
249 and carbonate units. In all lithologies, discontinuity orientation (bedding and joint sets) was
250 noted to be a controlling factor, creating planes of weakness within the rock mass resulting in
251 repeated rock slope failure. Cubic blocks of mudstone, measuring up to approx. 1.0 m in
252 length, occur on talus slopes beneath cliffs exhibiting fresh block failure scars. These blocks
253 occasionally displayed multiple internal fractures along parallel planes; the orientation of
254 these fractures mirrors the failure planes that bound the toppled blocks, suggesting consistent
255 structural weaknesses exist within the bedrock terrace above (Figure 3e). In carbonate units,

256 perpendicular vertical to subvertical joint sets (orientations estimated using the ROV
257 navigation data), result in small (approx. 0.2-0.5 m) wedge block failures where bedding
258 planes dipped out of the face of the rockwall (Figure 3f). Failure along these exposed
259 laterally continuous bedrock ledges resulted in a “saw-tooth” profile and associated ≤ 0.5 m
260 diameter diamond-shaped detachment blocks around the base of the ledge.

261 The mode of failure appears to be predominantly lithologically controlled, as spalling
262 and block failures were noted at various water depths (i.e. differing pressure and temperature
263 gradients) and in areas of varying hydrodynamic conditions (e.g. current velocities).

264 Examples of canyon wall erosion within mudstone units were chiefly noted at water depths of
265 between 850 – 1050 mbsl, with block failures of carbonate ledges noted at approx. 750 mbsl
266 and spalling/exfoliation of chalk cliff faces noted between approx. 2,000 – 3,500 mbsl. It is
267 likely that these failure mechanisms mainly reflect the physical properties of the stratigraphic
268 units exposed in the canyon rock wall at these depths, and external factors (e.g. water
269 temperature) play a reduced role in rock slope erosion.

270 Although large-scale rock slope failures (RSF) were not the main focus of this study,
271 boulder fields were observed, particularly towards the thalweg of the canyon. These typically
272 consisted of subrounded to subangular boulders (often >1.0 m in axial length) of mixed
273 lithologies, embedded within the canyon floor sediments suggesting sufficient time has
274 passed for this buildup of sediments to occur post-failure (Figure 4a & b). As many of these
275 large clasts were in contact with adjacent boulders (as opposed to overlying), and embedded
276 to similar depths within canyon floor sediments, this would suggest that the failure of each
277 block occurred simultaneously or within a short timeframe. However, as no rock avalanche
278 scars were observed in the canyon walls above, it is not possible to conclusively state whether
279 these boulders were deposited during one catastrophic failure event or are the result of
280 continued (and possibly ongoing) individual toppling failure episodes.

281

282

FIGURE 4 – HALF PAGE (FIGURE AND CAPTION AT END OF

283

MANUSCRIPT)

284

285

4.2 LABORATORY TEST RESULTS

286

287

288

289

290

291

292

293

294

295

The carbonate rock samples could be roughly divided into two groups based on appearance; fine to medium grained, white to yellowish grey on weathered surfaces, with open, smooth, irregular voids and no evidence of secondary carbonate precipitation. These samples were possibly oolitic and also fragmentary on weathered surfaces. Carbonate samples from the second group were fine to medium grained, very light grey to dark yellowish orange on weathered surfaces, massive with no obvious void spaces and no internal structure, and fragmentary on weathered surfaces. Samples from this group were noted to be muddier than those of the white carbonate group, in both appearance and texture. The unconsolidated sediment sample (soil in engineering terms) was identified as a silty clay through particle size analysis (Figure 5a).

296

297

298

299

300

301

The strength experiments revealed two distinct groups of carbonate rock: the muddy carbonates group which has a lower porosity and a higher strength than the pure carbonates group by a factor of about three and two to eight, respectively (Table 1 and Figure 5b). The muddy carbonates are classified as high to very high strength rocks while the pure carbonates are low to medium strength (Figure 5c) (Broch & Franklin, 1972). No clear effect on the mechanical strength could be related to the saturation condition (Figure 5b).

302

303

The plasticity plot (Figure 5d) shows the unconsolidated silty clay to be highly plastic.

304

TABLE 1 – FULL PAGE (END OF MANUSCRIPT WITH CAPTION)

305

306 **FIGURE 5 – HALF PAGE (FIGURE AND CAPTION AT END OF**
307 **MANUSCRIPT)**

308
309 **4.3 INFLUENCE OF BENTHOS ON CANYON SLOPE STABILITY**

310 Prominent features of the surveyed mudstone terraces included shallow borings (up to
311 approx. 2 cm diameter) and approx. 5-10 cm diameter burrows caused by benthic organisms,
312 often clustered into highly concentrated areas (Figure 4c & d).

313 Spalling and exfoliation is prevalent where terrace surfaces have been extensively
314 bored and it was noted that fresh surfaces exposed following spalling failure were devoid of
315 borings whereas adjacent, weathered surfaces were heavily bioeroded (Figure 4c).

316 In addition to the shallow borings, rows of adjacent burrows were noted along the
317 base of mudstone cliffs and terraces (up to 10 cm in diameter). These often appeared to
318 penetrate into the strata to depths exceeding 10 cm, although it was not possible to ascertain
319 maximum penetration depths within the terrace. Burrows were often situated within 20-50
320 cm of each other, resulting in sections of the base of terraces being gradually undermined.

321 Bioindicators of mass wasting were present across the canyon walls. These included
322 sections of carbonate ledges and walls where the absence of coral and other sessile fauna may
323 potentially highlight relatively recent spalling and block failures. Similar indicators were
324 visible on slopes completely dominated by coral communities, where failure of poorly
325 consolidated mudstone resulted in visible scars devoid of any benthic colonies.

326
327 **5. DISCUSSION**

328 Observations and data gathered during the CODEMAP 2015 research cruise to the
329 Whittard Canyon clearly illustrate the influence that both lithology and biological activity
330 may have upon rates of bedrock erosion over relatively short timescales.

331 **5.1 LITHOLOGICAL CONTROLS ON ROCK SLOPE EROSION**

332 Multiple instances of spalling failure were noted, which appeared to have the greatest
333 influence on cliffs and terraces composed of mudstone units. This differs from other
334 geographical locations where spalling failure has been documented in similar marine
335 environments; for instance, this process has been observed in submarine canyons along the
336 U.S. Atlantic Continental Margin by Chaytor *et al* (2016), where it mainly affected
337 carbonate-rich and chalk lithologies, and not mudstone terraces as is the case in the Whittard
338 Canyon. Observations also suggest that spalling failure and erosion of mudstone terraces
339 may influence the stability of overlying stratigraphic units. Where active mudstone terrace
340 retreat is occurring beneath more competent bedrock units (e.g. carbonates), and where
341 undermining along the base of terraced slopes is taking place, there is often an increase in
342 internal stresses within the overlying formation; this is known to result in rockfalls and
343 toppling failures onshore (Highland and Bobrowsky, 2008), and is likely to also be true for
344 the cases observed within the Whittard Canyon.

345 Block failures are controlled by inherent structural weaknesses within the bedrock
346 units, clearly visible in the form of perpendicular joint sets. Blocks of both mud and
347 carbonate lithologies were observed at the base of bedrock terraces where bedding planes
348 were noted to dip out of the cliff face. These blocks exhibited similar geometries (size and
349 orientation of surfaces), suggesting that regularly spaced joint sets are a common feature of
350 the stratigraphic units forming the bedrock terraces.

351 Onshore, rock strength is known to be critical for the stability of rock slopes with
352 outward dipping bedding planes, as the roughness of the joint provides frictional resistance
353 against failure (Selby, 1982). As the geotechnical results revealed that the pure carbonate
354 units were of weak to medium strength, the shearing of asperities along these joints due to
355 slope loading or increased stresses associated with bioerosion may result in the loss of

356 frictional resistance and subsequently block failure. Rock slope failures from steep carbonate
357 cliffs are not unknown; Paull *et al* (1990a) reported on fresh rock surfaces across the Florida
358 Escarpment which they linked with episodic collapse of the limestone terraces, highlighting
359 that subaqueous carbonate cliffs are still subjected to active erosion and modification at this
360 present time.

361 In carbonate lithologies, dissolution along joints, caused by the expulsion of
362 formation fluids, has been linked with initiating block failure by reducing the frictional
363 resistance along discontinuities in submerged rock slopes (McHugh *et al.*, 1993). Chemical
364 weathering of joints through spring sapping has even been proposed as a model for canyon
365 formation (e.g. Robb, 1984; Paull *et al.*, 1990b), illustrating the erosive potential of fluid
366 expulsion and migration along major joints and faults. This form of biochemical weathering
367 is challenging to identify at individual discontinuity resolution using ROV footage, however
368 aperture widths of >1 cm were noted within carbonate outcrops and karstic features that are
369 typically indicative of dissolution and fluid flow were observed in chalk units.

370 In addition, the geotechnical testing results show that the strength of the carbonate
371 units varies considerably depending on the apparent fine particle content; as the mud content
372 appears to increase (based on visual descriptions of the samples), pore spaces are reduced and
373 the carbonate unit becomes stronger. Shallow exfoliation and spalling of carbonate units may
374 be more prevalent across these weaker, purer carbonate lithologies where the internal shear
375 strength can be exceeded by external forces such as loading and drag from attached sessile
376 fauna. Block failure scars were numerous in areas of visibly porous, weak carbonate ledges
377 that were often densely populated by large communities of the clam *Acesta excavata* and
378 associated cold-water corals, adding additional stress through gravitational and drag forcing
379 which acts upon the intrinsically weak lithology.

380 It is difficult to determine why spalling and exfoliation erosion is so prevalent across
381 the lithological units of the Whittard Canyon. The McHugh *et al* (1993) study into the role of
382 diagenesis in exfoliation of carbonate units within submarine canyons of the U.S. Atlantic
383 Continental Margin links the fracturing of bedrock with the volume reduction of silica-rich
384 chalks, driven by fluid expulsion during progressive burial. As overburden is removed
385 during canyon incision and mass wasting processes, the diagenetically formed fractures
386 expand and exfoliation can occur (McHugh *et al.*, 1993). As failure is induced by loss of
387 support, stress release continues and erosion in the form of spalling and block failures can
388 occur on the exposed, fractured rock surface (McHugh *et al.*, 1993). In this way, a continual
389 cycle of terrace and cliff face erosion is maintained, and provides a plausible model for the
390 exfoliation of carbonate units within the Whittard Canyon.

391 Due to the highly plastic nature (atterberg limits of samples JC125_060_#1; Figure 1)
392 and the high clay content of the sampled soil, shrink-swell behavior was considered as a
393 factor for spalling of mudstone surfaces within the study area. However, the marine
394 environment under which these sediments were deposited and incised should prevent such
395 phenomenon as the clay should not shrink/swell due to it being in a fully saturated state. The
396 potential for shrink-swell to occur would remain if these clays are bearing some non-saline
397 water and this is exchanged for salt water. However, even if this were to occur, the effect on
398 the volume would likely remain very small. For these reasons, shrink-swell has been
399 discounted as being a major controlling factor on the observed spalling failure of mudstone
400 terraces/cliffs.

401 The single clay sample (JC125_060_#1) represents an unconsolidated sediment
402 terrace as opposed to a bedrock terrace, and therefore it does not give an accurate
403 representation of the weak mudstone terraces observed elsewhere in the canyon. It is
404 pertinent that the ROV failed to acquire a consolidated mudstone sample from the observed

405 bedrock terraces, due to the brittle nature of the available material, as this indicates the
406 general weak state of the mudstone units surveyed.

407 **5.2 EXTERNAL INFLUENCES ON BEDROCK EROSION**

408 Other factors that may influence bedrock slope erosion include the local
409 hydrodynamics, whereby current velocities exert increased shear stresses upon the base and
410 surfaces of vertical walls, promoting undercutting processes and shallow quarrying of the
411 exposed outcrops (Mitchell *et al.*, 2013; Mitchell, 2014). However, as the studies by Mitchell
412 *et al* (2013) and Mitchell (2014) highlight, bed shear stresses typically need to exceed 100 Pa
413 before quarrying and plucking of jointed bedrock can occur and would therefore be unlikely
414 to take place in the Whittard Canyon if relying exclusively on mean current velocities alone.
415 Mitchell (2006; 2014) did observe that sediment flows may well produce the bed shear
416 stresses required to initiate plucking and quarrying of bedrock within a canyon system, and
417 turbidity currents are known to occur within the Whittard Canyon system (e.g. Cunningham
418 *et al.*, 2005).

419 Burrowing and boring faunal communities also play an active role in spalling failure
420 within the Whittard canyon; it is likely that clusters of multiple borings are responsible for
421 creating a plane of weakness subparallel to the exposed surface, controlled by the depth at
422 which the organisms have excavated. This would result in a reduction in the rock mass
423 strength, leading to failure (Hecker, 1982). Chaytor *et al* (2016) noted the same phenomenon
424 in carbonate-rich lithologies within canyons along the U.S. Atlantic Continental Margin
425 where the failure depth of surface material appeared to be controlled by the depth of
426 bioerosion. Burrows and borings of a similar nature have been reported in exposed mudstone
427 units in the Monterey Canyon, California, leading to bioerosion of the bedrock slope (Paull *et*
428 *al.*, 2005). Burrows along the base of mudstone terraces, similar to those identified by Dillon

429 and Zimmerman (1970), also effectively undermine the material above, leading to a decrease
430 in the internal strength within the rock mass, which in turn would exacerbate terrace collapse.

431 Analysis of the video footage suggests that sessile fauna may also influence bedrock
432 erosion within the Whittard Canyon. In areas of block failures and shallow exfoliation
433 surfaces associated with the carbonate units, additional loading may be applied to the
434 terrace/cliff face through the erosive actions of sessile organisms. This can lead to an
435 increase in drag and gravitational forces (Hecker, 1982), and could be especially pertinent
436 within areas of the significantly weaker, pure carbonates. Sample L1, which produced very
437 low to medium strength point load results (I_{s50} 0.051 – 0.460), was noted to be heavily
438 encrusted with coral and other sessile organisms upon recovery from the base of the rock
439 slope.

440 The bedrock erosion mechanisms observed during expedition JC125 have
441 implications that extend beyond the area of the Whittard Canyon. While it is widely
442 documented that slope processes around the Celtic Margin include active erosion of margin
443 slopes, to-date studies have had a singular focus on unconsolidated sediment processes (e.g.
444 Cunningham *et al.*, 2005; Leynaud *et al.*, 2009). Evidence of spalling and block failure
445 across multiple exposed lithologies demonstrates ongoing erosion of the stratigraphic bedrock
446 framework upon which the NE Atlantic Continental Margin sediments are draped. Given that
447 the vast majority of the strata recovered in boreholes around the shelf and slope (e.g. Figure
448 2) are of carbonate or mud/clay composition, a significant proportion of the exposed bedrock
449 terraces/cliffs along the Celtic Margin is likely to be susceptible to the aforementioned
450 mechanisms of failure. This would suggest that the exposed bedrock cliffs and terraces are in
451 fact active and not inert features of the margin slopes.

452 Chaytor *et al* (2016) used the presence (and absence) of slow growing corals and
453 sponges to demonstrate long-term stability of canyon rockwalls and relative timings of rock

454 slope failures across canyons of the U.S. Atlantic Continental Margin. While no baseline
455 data is available to ascertain rates of erosion, the observed failure surfaces exhibited clear
456 fresh, and therefore relatively recent, scars and slopes were often devoid of benthic
457 communities implying recolonization had probably not taken place yet. Many erosional
458 scars, which were fresh in appearance with no benthic faunal communities attached, were
459 surrounded by well-established coral communities suggesting relatively recent failure of the
460 slope surface. In relation to the wider Celtic Margin and Whittard Canyon system, the large-
461 scale sediment slumps that have been documented are singular events that are likely to be
462 relatively infrequent when compared with the bedrock erosional processes.

463 The spalling of bedrock terraces and structurally-controlled block failures, coupled
464 with the geotechnical laboratory results, suggest that morphological alteration of the
465 rockwalls that underpin the Whittard Canyon is currently ongoing. In addition,
466 morphological modification of rock slopes through bioerosion was noted across several ROV
467 dives. A limited number of studies have noted these erosional processes in submarine
468 canyons across both active and passive margins elsewhere; Chaytor *et al* (2016) highlighted
469 the presence of similar spalling failures associated with clusters of borings in carbonate units
470 forming submarine canyon rockwalls across the U.S. Atlantic Continental Margin, and Paull
471 *et al* (2005) reported on notches, small caves and burrows penetrating and modifying
472 mudstone slopes that had become exposed through the mass wasting of overlying sediments
473 within the Monterey Canyon, California. This would suggest that these processes have wide
474 implications for the stability of submarine canyon rockwalls on a global scale. Furthermore,
475 research undertaken by Paull *et al* (1990a) on the Florida Escarpment also highlights that
476 these erosional processes influence the morphology of subaqueous bedrock slopes in different
477 geological settings and are therefore not only limited to rockwalls within submarine canyons.

478 Further work to better define the contribution of these small-scale processes on
479 canyon evolution, which have been underestimated until the present day is still required,
480 especially in relation to the physical properties of bedrock units. In addition, further studies
481 on the influence of benthic fauna on the modification of rock slope morphology within
482 submarine canyons would be beneficial. At present, the role that rock slope erosion has upon
483 sediment transfer and quantitative budgets within submarine canyons has not been
484 determined, and this should also be investigated further.

485

486 **6. CONCLUSIONS**

487 ROV observations coupled with geotechnical laboratory measurements have allowed
488 for a detailed assessment of the Whittard Canyon rockwalls to be undertaken. The following
489 conclusions can be drawn; (1) Ongoing spalling erosion is prevalent throughout the canyon,
490 particularly affecting brittle mudstone units. This process results in the build-up of
491 substantial talus slopes at the base of eroding terraces, and may lead to the undermining of
492 more competent units above; (2) Block failures within carbonate units are controlled by the
493 orientation of discontinuity joint sets, in addition to intrinsic strength properties which appear
494 to be influenced by the fine mud content (and therefore the available pore space) of the
495 lithology and; (3) Benthic organisms have the potential to exacerbate slope erosion in several
496 ways, and evidence of ongoing bioerosion was observed across mudstone and carbonate
497 lithologies.

498 Due to a lack of published data relating to submarine canyon rockwalls, it is
499 impossible to confirm that these erosional processes also occur at similar rates and with
500 similar results in submarine canyons worldwide. However, some of the processes described
501 above have been noted in canyons along the U.S. NW Atlantic Margin (Chaytor *et al.*, 2016)
502 and within the Monterey Canyon, California (Paull *et al.*, 2005). Our results highlight the

503 requirement for further studies to assess the contribution of the observed processes in canyon
504 evolutionary models and to better understand the interactive processes between benthic
505 communities and mass failure within submarine canyons.

506

507 **ACKNOWLEDGEMENTS**

508 This work was made possible by the CODEMAP 2015 research expedition to the
509 Whittard Canyon, Celtic Margin (funded by ERC Starting Grant 258482 and the NERC
510 MAREMAP programme). A special thank you to all members of the CODEMAP 2015
511 science team, and the captain and crew of the *RRS James Cook*. Gareth Carter publishes with
512 permission of the Director of the British Geological Survey (Natural Environment Research
513 Council). The authors would like to extend their sincerest gratitude to the reviewers
514 (Katherine Maier, United States Geological Survey, and Neil Mitchell, University of
515 Manchester, UK) and the Guest Editor (Pere Puig, Spanish National Research Council) for
516 their hugely constructive and encouraging feedback and comments on this manuscript. The
517 authors are also grateful to Emrys Phillips, British Geological Survey, for internal review of
518 the manuscript before submission.

519

520 **REFERENCES**

521 Amaro, T., Huvenne, V. A. I., Allcock, A. L., Aslam, T., Davies, J. S., Danovaro, R.,
522 De Stigter, H. C., Duineveld, G. C. A., Gambi, C., Gooday, A. J., Gunton, L. M., Hall, R.,
523 Howell, K. L., Ingels, J., Kiriakoulakis, K., Kershaw, C. E., Lavaleye, M. S. S., Robert, K.,
524 Stewart, H., Van Rooij, D., White, M. and Wilson, A.M. (2016). The Whittard Canyon – A
525 case study of submarine canyon processes. *Progress in Oceanography*, 146, 38–57.

526 Aslam, T., Hall, R. A., & Dye, S. R. (2017). Internal tides in a dendritic submarine
527 canyon. *Progress in Oceanography*.

528 ASTM Standard D2938-95, 2002, Standard Test Method for Unconfined
529 Compressive Strength of Intact Rock Core Specimens: ASTM International, West
530 Conshohocken, PA, www.astm.org.

531 ASTM Standard D3148-02, 2002, Standard Test Method for Elastic Moduli of Intact
532 Rock Core Specimens in Uniaxial Compression: ASTM International, West Conshohocken,
533 PA, www.astm.org.

534 ASTM Standard D4318-10, 2000, Standard test methods for liquid limit, plastic limit,
535 and plasticity index of soils: ASTM International, West Conshohocken, PA, www.astm.org.

536 ASTM Standard D4543-04, 2004, Standard Practices for Preparing Rock Core
537 Specimens and Determining Dimensional and Shape Tolerances: ASTM International, West
538 Conshohocken, PA, www.astm.org.

539 ASTM Standard D5731–5795, 2001, Standard method for determination of the point
540 load strength index of rock: ASTM International, West Conshohocken, PA, www.astm.org.

541 Broch, E. and Franklin, J. A. (1972). The point-load strength test. *International*
542 *Journal of Rock Mechanics and Mining Sciences & Geomechanics Abstracts*, 9, 669–676.

543 Chaytor, J. D., Demopoulos, A. W. J., ten Brink, U. S., Baxter, C., Quattrini, A. M.
544 and Brothers, D. S. (2016). Assessment of Canyon Wall Failure Process from Multibeam
545 Bathymetry and Remotely Operated Vehicle (ROV) Observations, U.S. Atlantic Continental
546 Margin. In G. Lamarche, J. Mountjoy, S. Bull, T. Hubble, S. Krastel, E. Lane, A. Micallef, L.
547 Moscardelli, C. Mueller, I. Pecher, and S. Woelz (Eds.), *Submarine Mass Movements and*
548 *their Consequences*, 7th *International Symposium* (pp. 103–113). Switzerland, Springer
549 International Publishing.

550 Cunningham, M. J., Hodgson, S., Masson, D. G. and Parson, L. M. (2005). An
551 evaluation of along-and down-slope sediment transport processes between Goban Spur and
552 Brenot Spur on the Celtic Margin of the Bay of Biscay. *Sedimentary Geology*, 79(1), 99–116.

553 Dillon, W. P. and Zimmerman, H. B. (1970). Erosion by biological activity in two
554 New England submarine canyons. *Journal of Sedimentary Research*, 40(2), 542-547.

555 Evans, C. D. R. and Hughes, M. J. (1984). The Neogene succession of the South
556 Western Approaches, Great Britain. *Journal of the Geological Society*, 141(2), 315–326.

557 Evans, C. D. R. (1990) *The geology of the western English Channel and its western*
558 *approaches*. London, HMSO for the British Geological Survey, 93 p.

559 Fairhurst, C. E. and Hudson, J. A. (1999). Draft ISRM suggested method for the
560 complete stress-strain curve for intact rock in uniaxial compression, ISRM suggested
561 methods (SMs): second series. *International Journal of Rock Mechanics and Mining*
562 *Sciences*, 36, 279–289.

563 Franklin, J. A. (1985). Suggested method for determining point load strength, ISRM
564 suggested methods. *International Journal of Rock Mechanics and Mining Sciences &*
565 *Geomechanics Abstracts*, 22, 51–60.

566 Hall, R. A., Aslam, T., & Huvenne, V. A. (2017). Partly standing internal tides in a
567 dendritic submarine canyon observed by an ocean glider. *Deep Sea Research Part I:*
568 *Oceanographic Research Papers*.

569 Hecker, B. (1982). Possible benthic fauna and slope instability relationships. In S.
570 Saxov and J. K. Nieuwenhuis (Eds.), *Marine Slides and Other Mass Movements* (pp. 335–
571 347). New York, Plenum.

572 Highland, L. and Bobrowsky, P. T. (2008). The landslide handbook: a guide to
573 understanding landslides (p. 129). Reston, U.S. Geological Survey.

574 Huvenne, V. A. I., Wynn, R. B. and Gales, J. A. (2016). RRS James Cook Cruise 124-
575 125-126. CODEMAP2015: Habitat mapping and ROV vibrocorer trials around Whittard
576 Canyon and Haig Fras. National Oceanography Centre Open-File Report (Cruise Report No.
577 36).

578 Leynaud, D., Mienert, J. and Vanneste, M. (2009). Submarine mass movements on
579 glaciated and non-glaciated European continental margins: a review of triggering
580 mechanisms and preconditions to failure. *Marine and Petroleum Geology*, 26(5), p. 618–632.

581 Lo Iacono, C., Sulli, A., Agate, M., Lo Presti, V., Pepe, F. and Catalano, R. (2011).
582 Submarine canyon morphologies in the Gulf of Palermo (Southern Tyrrhenian Sea) and
583 possible implications for geo-hazard. *Marine Geophysical Research*, 32(1-2), 127–138,
584 doi:10.1007/s11001-011-9118-0.

585 McHugh, C. M., Ryan, W. B. and Schreiber, B. C. (1993). The role of diagenesis in
586 exfoliation of submarine canyons. *AAPG Bulletin*, 77(2), 145-172.

587 Micallef, A., Mountjoy, J. J., Canals, M. and Lastras, G. (2012). Deep-seated bedrock
588 landslides and submarine canyon evolution in an active tectonic margin: Cook Strait, New
589 Zealand. In Y. Yamada, K. Kawamura, K. Ikehara, Y. Ogawa, R. Urgeles, D. Mosher, J.
590 Chaytor, and M. Strasser (Eds.), *Submarine Mass Movements and their Consequences*, 5th
591 *International Symposium* (pp. 201–212). Netherlands, Springer.

592 Mitchell, N. C. (2006). Morphologies of knickpoints in submarine canyons.
593 *Geological Society of America Bulletin*, 118(5-6), 589-605.

594 Mitchell, N. C., Huthnance, J. M., Schmitt, T. and Todd, B. (2013). Threshold of
595 erosion of submarine bedrock landscapes by tidal currents. *Earth Surface Processes and*
596 *Landforms*, 38(6), 627-639.

597 Mitchell, N. C. (2014). Bedrock erosion by sedimentary flows in submarine canyons.
598 *Geosphere*, 10(5), 892-904.

599 Montadert, L., Roberts, D. G., Auffret, G. A., Bock, W. D., Dupeuble, P. A.,
600 Hailwood, E. A., Harrison, W. E., Kagami, H., Lumsden, D. N., Muller, C. M., Schnitker, D.,
601 Thompson, R. W., Thompson, T. L., Timofeev, P. P., and Mann, D. (1979). Deep Sea
602 Drilling Project (DSDP), Site 402/Hole 402A, doi:10.2973/dsdp.proc.48.105.1979.

603 Paull, C. K., Freeman-Lynde, R., Bralower, T. J., Gardemal, J. M., Neumann, A. C.,
604 D'Argenio, B. and Marsella, E. (1990a). Geology of the strata exposed on the Florida
605 Escarpment. *Marine Geology*, 91(3), 177-194.

606 Paull, C. K., Spiess, F. N., Curray, J. R. and Twichell, D. C. (1990b). Origin of
607 Florida Canyon and the role of spring sapping on the formation of submarine box canyons.
608 *Geological Society of America Bulletin*, 102(4), 502-515.

609 Paull, C. K., Ussler, W., Greene, H. G., Barry, J. and Keaten, R. (2005). Bioerosion
610 by chemosynthetic biological communities on Holocene submarine slide scars. *Geo-Marine*
611 *Letters*, 25(1), 11-19.

612 Puig, P., Ogston, A. S., Mullenbach, B. L., Nittrouer, C. A., & Sternberg, R. W.
613 (2003). Shelf-to-canyon sediment-transport processes on the Eel continental margin (northern
614 California). *Marine Geology*, 193(1), 129-149.

615 Puig, P., Palanques, A., and Martín, J. (2014). Contemporary sediment-transport
616 processes in submarine canyons. *Annual review of marine science*, 6, 53-77.

617 Robb, J. M. (1984). Spring sapping on the lower continental slope, offshore New
618 Jersey. *Geology*, 12(5), 278-282.

619 Rowe, G. T. (1974). The effects of the benthic fauna on the physical properties of
620 deep-sea sediments. In A. Inderbitzen (Ed.), *Deep-Sea Sediments: Physical and Mechanical*
621 *Properties* (pp. 381–400). New York, Springer.

622 Scourse, J., Uehara, K., and Wainwright, A. (2009). Celtic Sea linear tidal sand
623 ridges, the Irish Sea Ice Stream and the Fleuve Manche: palaeotidal modelling of a
624 transitional passive margin depositional system. *Marine Geology*, 259(1), 102-111.

625 Selby, M. J. (1982). Controls on the stability and inclinations of hillslopes formed on
626 hard rock. *Earth Surface Processes and Landforms*, 7(5), 449-467.

627 Stewart, H. A., Davies, J. S., Guinan, J. and Howell, K. L. (2014). The Dangeard and
628 Explorer canyons, South Western Approaches UK: Geology, sedimentology and newly
629 discovered cold-water coral mini-mounds. *Deep Sea Research Part II: Topical Studies in*
630 *Oceanography*, 104, 230–244.

631 Sultan, N., Gaudin, M., Berne, S., Canals, M., Urgeles, R. and Lafuerza, S. (2007).
632 Analysis of slope failures in submarine canyon heads: an example from the Gulf of Lions.
633 *Journal of Geophysical Research: Earth Surface*, 112(F1), doi:10.1029/2005JF000408.

634 Sumner, E. J., Peakall, J., Dorrell, R. M., Parsons, D. R., Darby, S. E., Wynn, R. B.,
635 McPhail, S. D., Perrett, J., Webb, A., and White, D. (2014). Driven around the bend: Spatial
636 evolution and controls on the orientation of helical bend flow in a natural submarine gravity
637 current. *Journal of Geophysical Research: Oceans*, 119(2), 898-913.

638 Talling, P. J. (2014). On the triggers, resulting flow types and frequencies of
639 subaqueous sediment density flows in different settings. *Marine Geology*, 352, 155-182.

640 Ulusay, R. and Hudson, J. A. (2007). The complete ISRM suggested methods for rock
641 characterization, testing and monitoring: 1974-2006. In R. Ulusay and J. A. Hudson (Eds.),
642 *Commission on testing methods. International Society of Rock Mechanics. Compilation*
643 *arranged by ISRM Turkish National Group*. Turkey, Springer.

644 Valentine, P. C., Uzzmann, J. R. and Cooper, R. A. (1980). Geologic and biologic
645 observations in Oceanographer submarine canyon: descriptions of dives aboard the research
646 submersibles Alvin (1967, 1978) and Nekton Gamma (1974). *U.S. Geological Survey Open*
647 *File Report*, 80–76: 40 pp.

648 Warne, J. E., Slater, R. A. and Cooper, R. A. (1978). Bioerosion in submarine
649 canyons. In D. J. Stanley and G. Kelling (Eds.), *Sedimentation in submarine canyons, fans,*
650 *and trenches*. Stroudsburg, Pennsylvania, Dowden, Hutchinson and Ross, p. 65–70.

651

Sample ID	Sample Type	Depth (mbsl)	Latitude	Longitude	IS ₅₀
L1a	pure carbonate	-736.30	48.759976	-10.458456	0.263
L1b	pure carbonate	-736.30	48.759976	-10.458456	0.252
L1c	pure carbonate	-736.30	48.759976	-10.458456	0.223
L1d	pure carbonate	-736.30	48.759976	-10.458456	0.280
L1e	pure carbonate	-736.30	48.759976	-10.458456	0.209
L1f	pure carbonate	-736.30	48.759976	-10.458456	0.401
L1g	pure carbonate	-736.30	48.759976	-10.458456	0.079
L1h	pure carbonate	-736.30	48.759976	-10.458456	0.120
L1i	pure carbonate	-736.30	48.759976	-10.458456	0.333
L1j	pure carbonate	-736.30	48.759976	-10.458456	0.460
L1k	pure carbonate	-736.30	48.759976	-10.458456	0.100
L1l	pure carbonate	-736.30	48.759976	-10.458456	0.088
L1m	pure carbonate	-736.30	48.759976	-10.458456	0.073
L1n	pure carbonate	-736.30	48.759976	-10.458456	0.080
L1o	pure carbonate	-736.30	48.759976	-10.458456	0.051
L1p	pure carbonate	-736.30	48.759976	-10.458456	0.135
L1q	pure carbonate	-736.30	48.759976	-10.458456	0.081
L2a	pure carbonate	-491.50	48.737467	-10.090386	0.263
L2b	pure carbonate	-491.50	48.737467	-10.090386	0.306
L2c	pure carbonate	-491.50	48.737467	-10.090386	0.212
L2d	pure carbonate	-491.50	48.737467	-10.090386	0.366
L2e	pure carbonate	-491.50	48.737467	-10.090386	0.268
L2f	pure carbonate	-491.50	48.737467	-10.090386	0.245
L2g	pure carbonate	-491.50	48.737467	-10.090386	0.282
L2h	pure carbonate	-491.50	48.737467	-10.090386	0.211
L2i	pure carbonate	-491.50	48.737467	-10.090386	0.163
L3a	pure carbonate	-874.00	48.735818	-10.099441	0.121
L3b	pure carbonate	-874.00	48.735818	-10.099441	0.338
L4a	pure carbonate	-760.30	48.760368	-10.461013	0.345
#5a	muddy carbonate	-838.00	48.753295	-10.472528	2.382
#5b	muddy carbonate	-838.00	48.753295	-10.472528	2.527
#6a	muddy carbonate	-841.00	48.753296	-10.472546	3.045
#6b	muddy carbonate	-841.00	48.753296	-10.472546	2.608
#6c	muddy carbonate	-841.00	48.753296	-10.472546	2.729
#6d	muddy carbonate	-841.00	48.753296	-10.472546	2.064
#6e	muddy carbonate	-841.00	48.753296	-10.472546	0.845
#6f	muddy carbonate	-841.00	48.753296	-10.472546	2.716
#6g	muddy carbonate	-841.00	48.753296	-10.472546	2.364
#6h	muddy carbonate	-841.00	48.753296	-10.472546	2.233
#6i	muddy carbonate	-841.00	48.753296	-10.472546	0.585

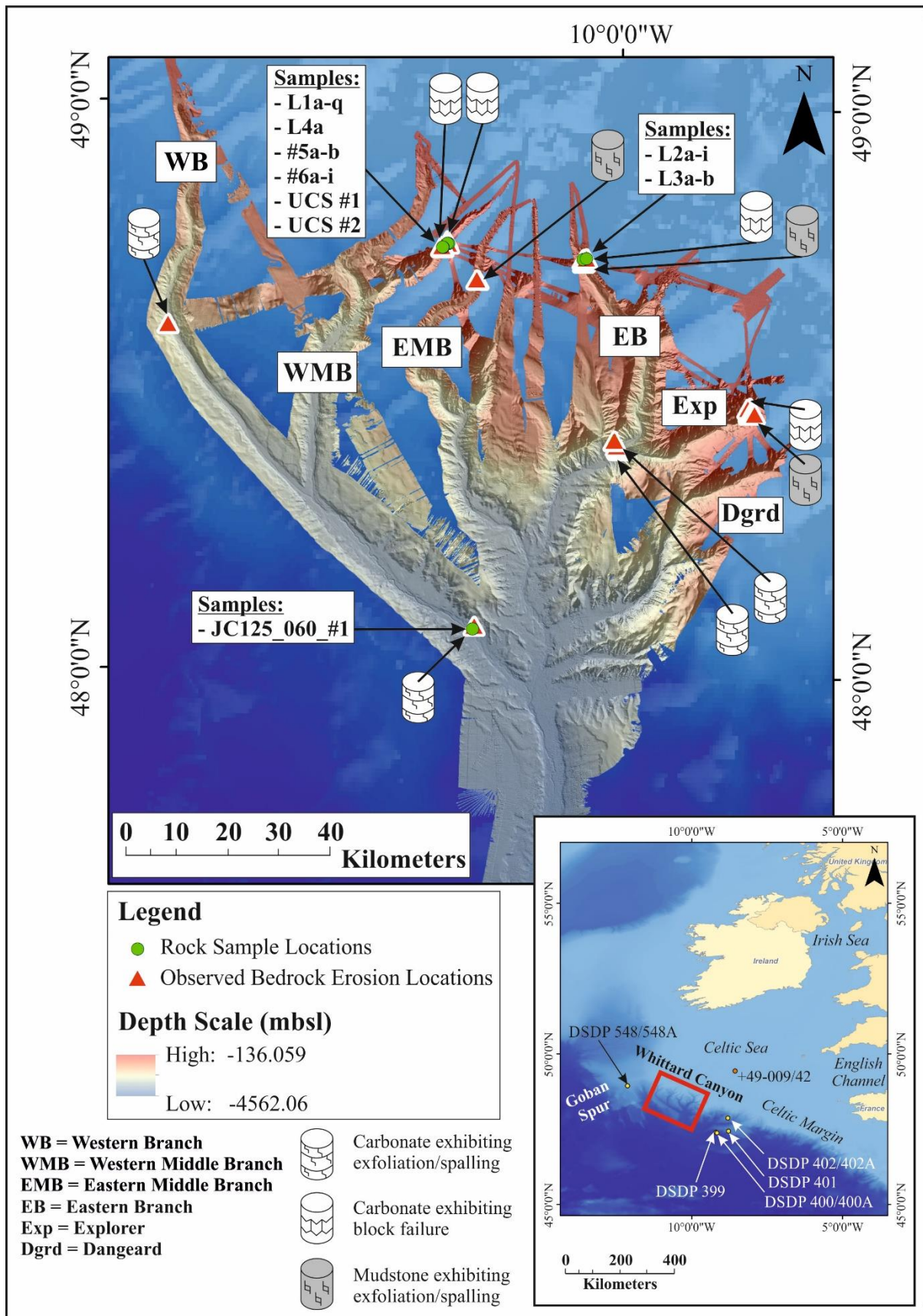
Table 1: Point Load Index (PLI) testing results, showing the difference in strength values between pure and muddy carbonate samples.

653
654

655

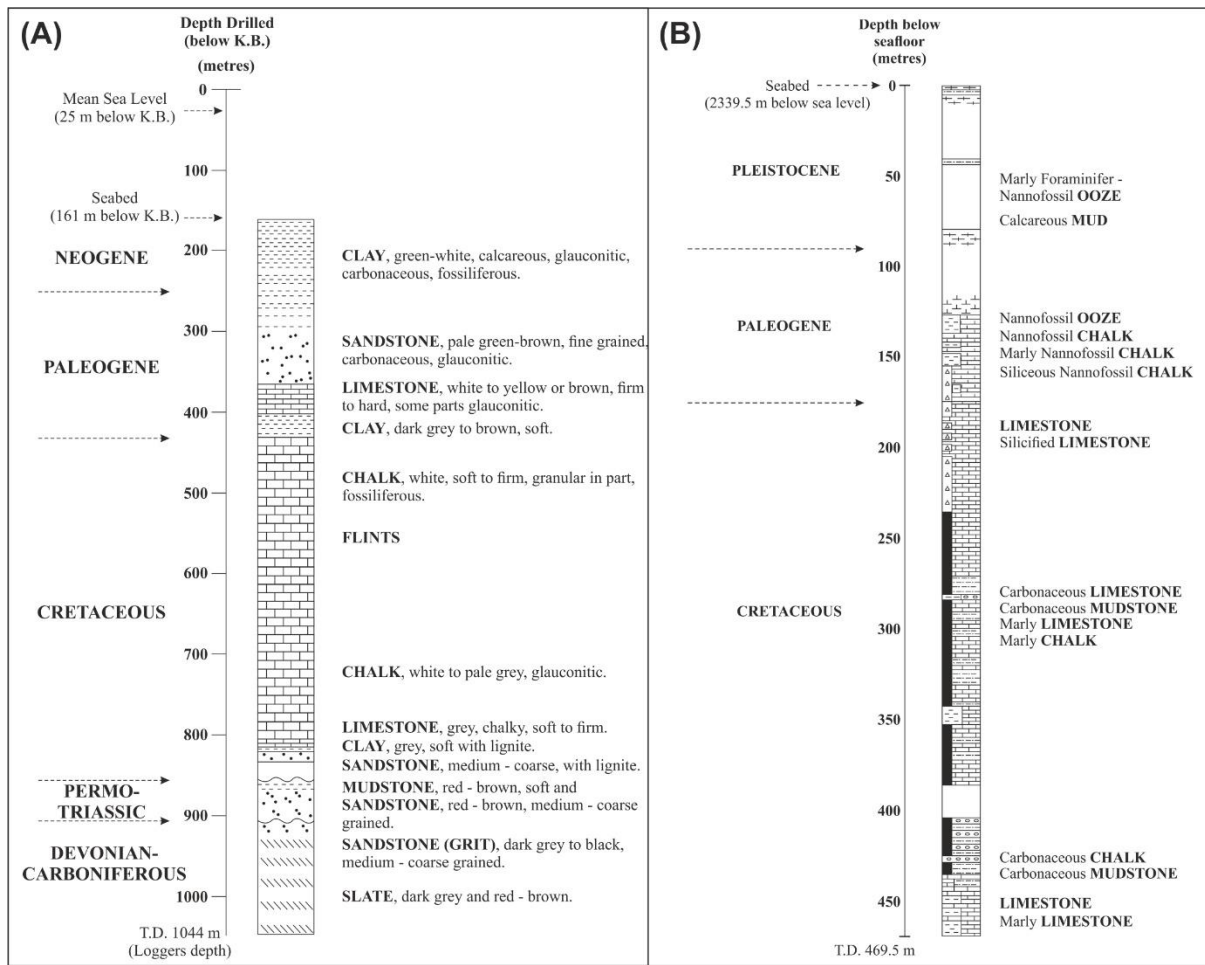
656

657



658

659 **Figure 1:** Location of study area (red box) is inset, with locations of boreholes displayed (orange dot for BGS borehole
 660 and yellow dots for DSDP boreholes). Main figure shows hillshaded bathymetric map of the Whittard Canyon gridded to
 661 50 m overlying GEBCO data. Locations of rock samples and bedrock erosion observations are shown.



662

663 **Figure 2: (A) BGS borehole +49-009/42 (K.B. Kelly Bushing) and (B) DSDP borehole 402, illustrating regional stratigraphy**
 664 **across the shelf and slope into which the Whittard Canyon is incised (adapted from Montadert *et al.*, 1979).**

665

666

667

668

669

670

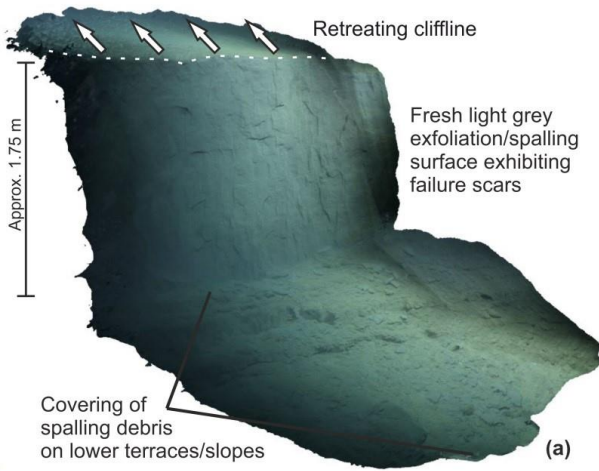
671

672

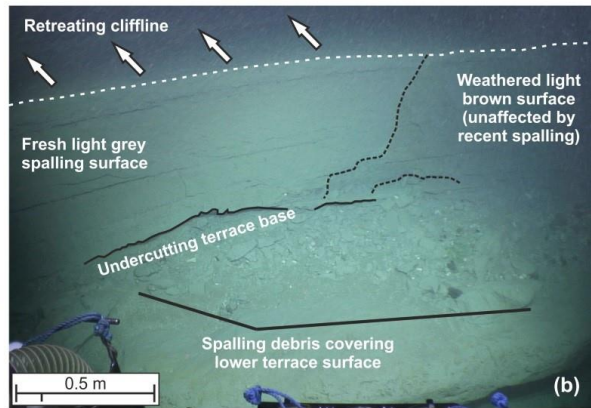
673

674

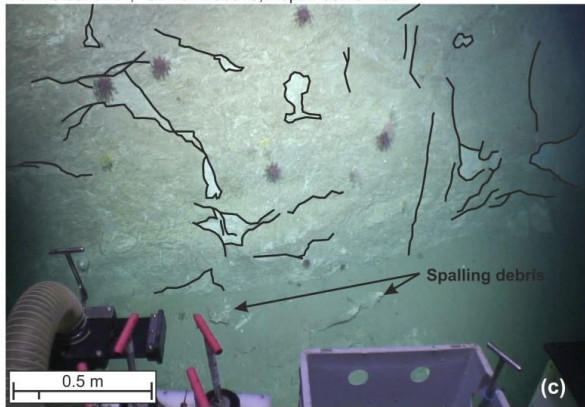
675



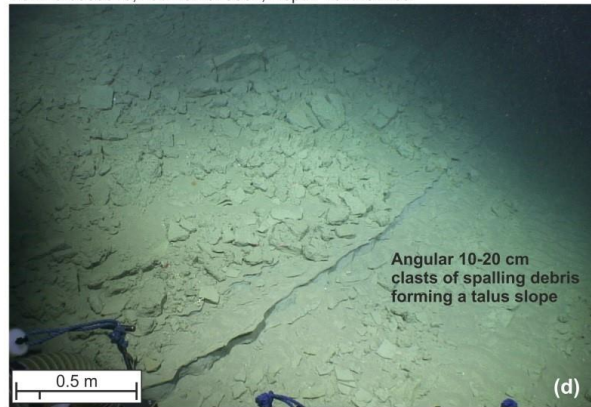
Lon: -9.6570247; Lat: 48.4756348; Depth: 852.6 mbsl



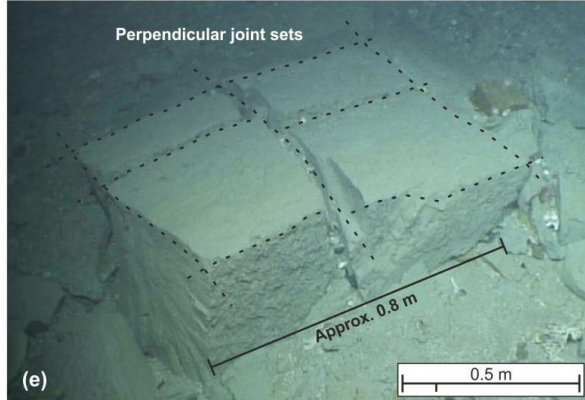
Lon: -9.6535018; Lat: 48.4675862; Depth: 1017.5 mbsl



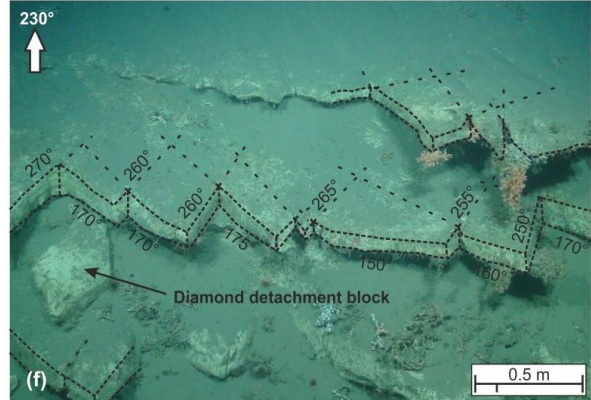
Lon: -11.199363; Lat: 48.6075657; Depth: 2617.1 mbsl



Lon: -9.6537852; Lat: 48.4693107; Depth: 1001.6 mbsl



Lon: -9.6534137; Lat: 48.4674213; Depth: 1030.5 mbsl



Lon: -10.4749982; Lat: 48.7530402; Depth: 740.0 mbsl

676

677

678

679

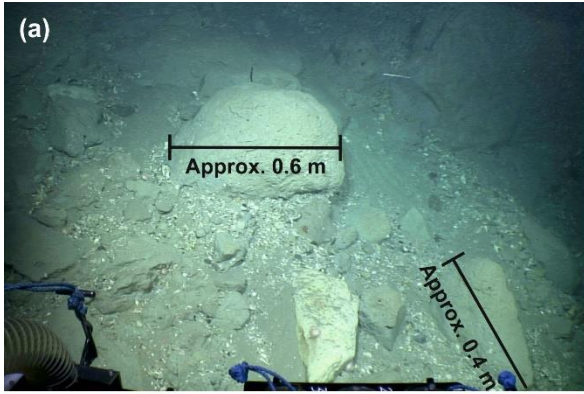
680

681

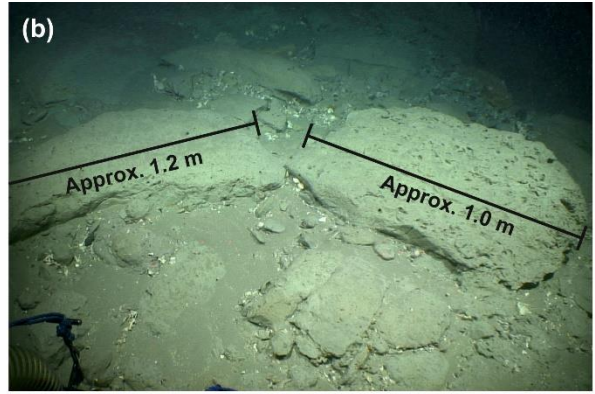
682

683

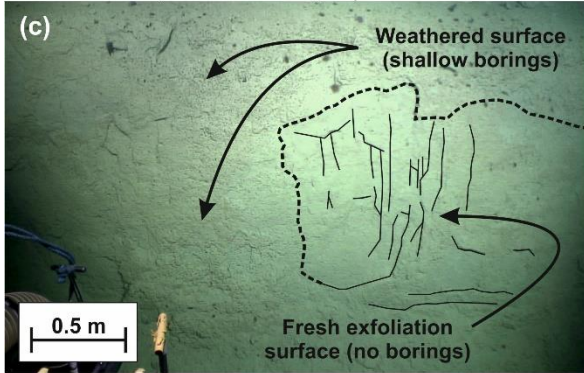
Figure 3: (a) & (b) show spalling/exfoliation surfaces on mudstone terraces, resulting in cliffline retreat; (c) exfoliation on a chalk cliff surface; (d) extensive accumulations of mudstone material at base of spalling terrace, forming a talus slope; and (e) & (f) show structurally controlled block failures in mudstone and carbonate units respectively.



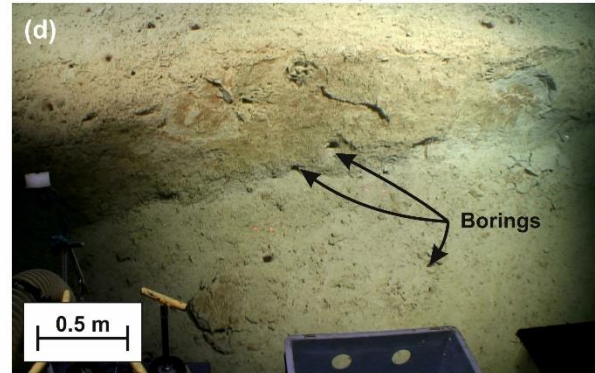
Lon: -9.6527113; Lat: 48.4660002; Depth: 1065.8 mbsl



Lon: -9.6527818; Lat: 48.4660627; Depth: 1064.8 mbsl



Lon: -9.639216; Lat: 48.465525; Depth: 736.2 mbsl



Lon: -9.6429888; Lat: 48.4673043; Depth: 864.2 mbsl

684

685

686

687

688

689

690

691

692

693

694

695

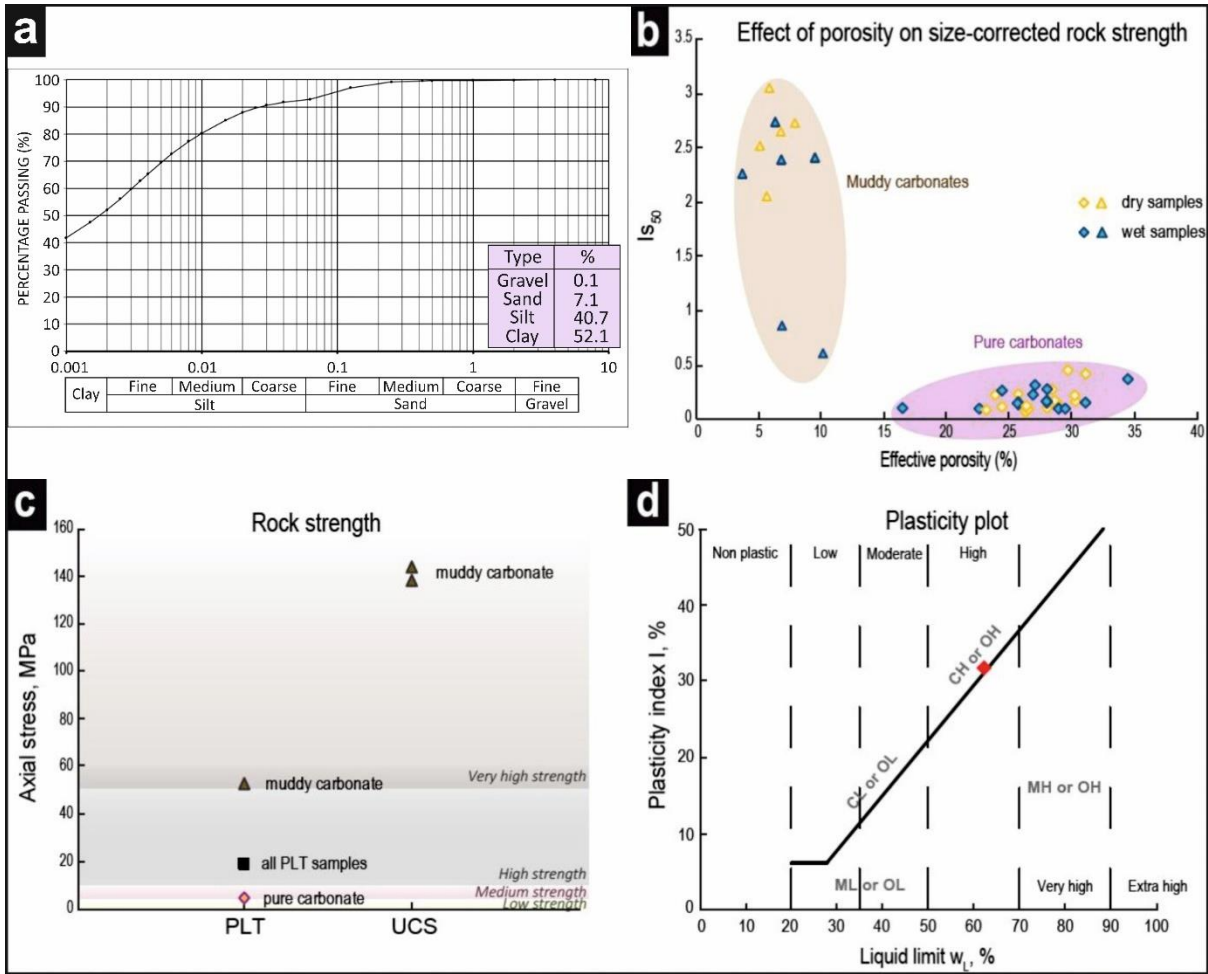
696

697

698

699

Figure 4: (a) & (b) boulders of mixed lithologies embedded in canyon floor sediments; (c) shallow borings cover the terrace surface to the left of the image, whereas the fresh, exfoliation surface is devoid of borings and; (d) larger borings penetrating a weathered mudstone terrace.



700

701 Figure 5: Summary of geotechnical results (a) grain size analysis of the unconsolidated sediment sample, showing it to be
 702 a silty clay; (b) effective porosity vs strength (c) rock strength (Point Load Test & Unconfined Compressive Strength) of
 703 pure carbonates and muddy carbonates (d) plasticity plot for silty clay sample.

704